Journal of Electroceramics 5:1, 37–51, 2000

Evaluating Dielectric Impedance Spectra using Effective Media Theories

D.S. McLACHLAN,[1,2] J.-H. HWANG[1] & T.O. MASON[1]

[1]*Department of Materials Science and Engineering, Northwestern University, Evanston, IL, 60208, USA*
[2]*Physics Department, University of the Witwatersrand, P.O. WITS 2050, Johannesburg, South Africa*

Submitted April 4, 1999; Revised July 14, 1999; Accepted November 23, 1999

Abstract. The immittance spectra (i.e., impedance and modulus representations) are calculated for various effective medium theories, i.e., the Maxwell-Wagner (MW), Hashin-Shtrikman (HS), Bruggeman Asymmetric (BA) and Bruggeman Symmetric (BS) models, with emphasis on their individual microstructures. In addition the brick-layer (BL) model is also considered. The BL and MW-HS models yield similar single impedance arcs for a relatively low volume fraction conductive matrix (coating on the low conductivity phase). The BA model yields single impedance arcs different from the MW-HS models. The BL and MW-HS models yield virtually identical dual impedance arc behavior for a low volume fraction insulating matrix (coating on the high conductivity phase). At low volume fractions of insulating matrix, the low frequency arc due to the insulating material for the BA model is much smaller than for the MW-HS model. The BS model exhibits single impedance arc behavior when the volume fraction of conductor is above or near the percolation threshold and dual arc behavior somewhat below the percolation threshold. Equivalent circuits for these model materials are discussed, and application is made to experimental data for various electroceramic systems.

Keywords: impedance spectroscopy, effective media theories, equivalent circuits, microstructure, grain boundaries

1. Introduction

Impedance spectroscopy is routinely used to characterize the electrical transport properties of ''composite'' electroceramics with heterogeneous microstructures. The simplest spectra to understand are for two component or phase systems where one component coats the other. The coating component should have a significantly lower or higher conductivity than the other. This component could be grain boundaries or a true second phase distributed uniformly at the interfaces of the granular component, and with continuous 3D connectivity; the volume fraction of the coating phase could range from very small to nearly one. Effective media (EM) theories can be used in both of these cases (conductive or insulating coating phase).

In other electroceramics, with a large contrast in the conductivities of the two components, a rapid change in the conductivity can be observed at the critical volume fraction where the conducting component changes from 0D to 3D connectivity. This can in some instances be described by the Bruggeman Asymmetric Media theory but more often by percolation theory. The IS spectra of percolation systems will be discussed in later publications.

This paper addresses the immittance (i.e., impedance and modulus) response of systems described by the classical effective media (EM) theories and how these relate to the underling microstructures. The standard EM theories include the Maxwell-Wagner (MW) (or Hashin-Shtrikman (HS)), Bruggeman Asymmetric (BA) and Bruggeman Symmetric (BS) models. In addition, the brick-layer model (BL) is also considered, since it is so frequently used to describe the behavior of grain boundary-controlled electroceramics. The MW-HS, BA, and BL equations all describe systems where one component coats the

other, while the BS equation applies to a percolation type microstructure. However, as it is an EM theory, it is included here for completeness and the BS impedance spectra are compared with those obtained from the other equations. An equivalent circuit analysis is applied to these mathematically well defined microstructures and important ramifications are discussed.

2. Effective Media Theories

Effective media theories from Maxwell to Maxwell-Wagner (MW) and on to the Bruggeman Symmetric (BS) and Bruggeman Asymmetric (BA) media and percolation theories are reviewed, up until 1979, by Landauer [1]. McLachlan et al. [2] also discussed these topics and introduced the one exponent General Effective Medium (GEM) equation. Merideth and Tobias [3] give a particularly thorough review of the MW, BA and related theories. For an in-depth discussion and derivation of these equations, more on anisotropic media and an introduction to percolation theory, the reader is referred to the review articles [1–9] and the references therein. References [4,5,9] deal primarily with percolation theories and structures, which are not covered in this article. Emphasis in this article will be placed on isotropic media, built up using spherical elements.

The various binary phase media, which have a complex conductivity σ_m^* (resistivity $\rho_m^* = 1/\sigma_m^*$), discussed in this section will all consist of two components, the highly conducting one with a conductivity of σ_h^* (resistivity $\rho_\ell^* = 1/\sigma_h^*$) and a more insulating one characterized by $(1/\sigma_\ell^* = \rho_h^*)$. In all equations, one can substitute the appropriate complex dielectric constant $(\varepsilon^* = \varepsilon_r + i\varepsilon_i)$, complex conductivity $(\sigma^* = \sigma_r + i\sigma_i)$, or complex permeability $(\mu^* = \mu_r + i\mu_i)$ for the equivalent σ_m, σ_h or σ_ℓ. If σ_h^* and/or σ_ℓ^* are functions of the angular frequency ω, all the equations for σ_m^* can be given as a function of ϕ for fixed ω or ω for fixed ϕ. The volume fraction of the more conductivity component is given by ϕ and the less by $f = 1 - \phi$.

The first effective media equations, due to Maxwell, for a dilute dispersion of spheres with $\sigma = \sigma_d$ (volume fraction V_d) in a matrix with $\sigma = \sigma_o$ and valid for $V_d < 0.1$ [3], are

$$\sigma_m = (\sigma_d + 2\sigma_o - 2V_d(\sigma_o - \sigma_d))/ (\sigma_d + 2\sigma_o + V_d(\sigma_o - \sigma_d)) \qquad (1a,b)$$

here either $\sigma_d = \sigma_\ell$ and $\sigma_o = \sigma_h$ or visa versa. In the limits of a perfect insulator $(\sigma_\ell = 0)$ or a perfect conductor $(\sigma_h = \infty)$ these equations become,

$$\sigma_m = \sigma_h\left(1 - \frac{3}{2}f\right) \text{ and } \rho_m = \rho_h(1 - 3\phi) \qquad (2a,b)$$

All valid effective media theories must reduce to these expressions in the dilute limit.

The well known Maxwell-Wagner relationships for spherical inclusions are

$$\frac{\sigma_m - \sigma_h}{\sigma_m + 2\sigma_h} = f\frac{\sigma_\ell - \sigma_h}{\sigma_\ell + 2\sigma_h} \text{ and } \frac{\sigma_m - \sigma_\ell}{\sigma_m + 2\sigma_\ell} = \phi\frac{\sigma_h - \sigma_\ell}{\sigma_h + 2\sigma_\ell} \qquad (3a,b)$$

A MW medium can be visualized as built up from a space-filling array of coated spheres, as illustrated in Fig. 1(b)(i) for Eq. (3a) and Fig. 1(b)(ii) for Eq. (3b). When assembled together, the coating component forms the matrix or host component (σ_h in Eq. (3a) and σ_ℓ in Eq. (3b)). Note that, as the coatings on the spheres persist until f or $\phi = 1$, there is no percolation

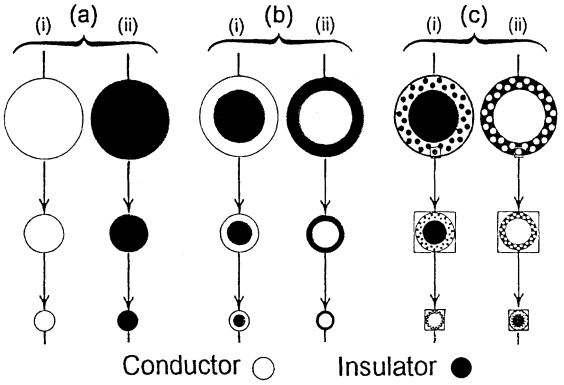

Fig. 1. This figure illustrates the building blocks for the microstructures which are characterized by (a). (i) & (ii) Bruggeman's Symmetric Media equation (Eq. (5)), (b). (i) & (ii) the Maxwell-Wagner equation (Eq. (3)) and (c). (i) & (ii) Bruggeman's Asymmetric Media equations (Eqs. (4)). Note that, as indicated in (a) and (b) by the progressively smaller coated spheres, these media require a very large range of sphere size. In (c) the second (third) coated sphere is an enlargement of the region surrounding a small sphere of the first (second) coated sphere.

threshold. $\phi_c = 0$ or 1 is not a percolation threshold, as the medium then consists of a single component. The Maxwell-Wagner equations are also equivalent to the Hashin-Shtrikman (HS) upper and lower bounds for the conductivity (resistivity) of an isotropic two component mixture and the Clausius-Mossetti equation for dielectrics. The microstructures, modeled by the Clausius-Mossotti and HS equations are the same as for the MW system. These equations are plotted as curves *b* in Fig. 2.

The Bruggeman asymmetric media equations, for spherical inclusions or grains, are [1–3],

$$\frac{(\sigma_m - \sigma_\ell)^3}{\sigma_m} = (1-f)^3 \frac{(\sigma_h - \sigma_\ell)^3}{\sigma_h} \text{ and}$$

$$\frac{(\sigma_m - \sigma_h)^3}{\sigma_m} = (1-\phi)^3 \frac{(\sigma_\ell - \sigma_h)^3}{\sigma_\ell} \qquad (4a,b)$$

The building ''blocks'' for the media described by Eq. (4a) are illustrated in column (c)(i) of Fig. 1, and for Eq. (4b) in column (c)(ii). The derivation of these equations also requires that there is a very large range of the building block or sphere sizes. Again there is a specific host or matrix component and no percolation threshold. These equations are derived in [1] and [3] and plotted as curves *c* in Fig. 2.

Bruggeman's symmetric medium equation for an isotropic medium, built up from a very large size range of the conducting and insulating spheres, shown in columns a(i) and a(ii) of Fig. 1, is

$$\phi(\sigma_h - \sigma_m)/(\sigma_h + A\sigma_m) + (1-\phi)$$
$$(\sigma_\ell - \sigma_m)/(\sigma_\ell + A\sigma_m) = 0 \qquad (5)$$

where $A = 2$ for this (spherical components) case. The randomly arranged, space-filling spheres shown in columns (a)(i) and (a)(ii) of Fig. 1 are randomly assigned to be conducting or non-conducting, so that a fraction ϕ of them have the higher conductivity (therefore $1-\phi$ or f of the spheres have the lower conductivity). References [2] and [3], and the references therein, give alternate expressions for *A*. A is derived from the demagnetization coefficients of the ellipsoids building up the model media, which can be made up out of either oriented or randomly oriented ellipsoids. For both model and ''real or continuum'' systems *A* always equals $(1-\phi_c)/\phi_c$, where ϕ_c is the critical volume fraction (percolation type threshold) at which the conducting component first forms a continuous path.

Note that an ideal effective medium is one in which each sphere (ellipsoid) is surrounded by a mixture of the two components that has the mean or effective

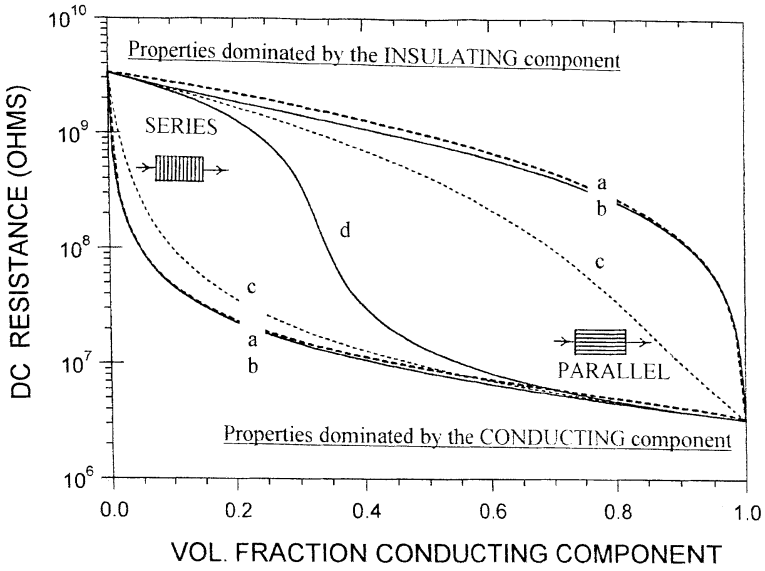

Fig. 2. Resistivity bounds for two component media as a function of volume fraction. One component has a resistivity $\rho_h = 3.33 \times 10^9$ ohm-m ($\sigma_l = 3 \times 10^{-8}$) and the other $\rho_l = 3.33 \times 10^6$ ohm-m ($\sigma_h = 3 \times 10^{-5}$). The curves are (a) the brick-layer model (Eq. (6)), (b) the Maxwell-Wagner equations (Eqs. 3a,b) or the Hashin-Shtrikman upper and lower bounds (c) the Bruggeman Asymetric Equations (Eqs. (4a,b)), and (d) the Bruggeman Symmetric Equation (Eq. (5)).

value for the medium. This requires that the dispersed spheres (ellipsoids) have an effectively infinite range in size, and that the larger spheres are separated by material containing smaller spheres. It is not valid near a percolation threshold, where spheres (ellipsoids) of similar size come, or nearly come, into contact with each other [10]. In practice, effective media theories work best for lower values of f or ϕ, where the dispersed spheres (ellipsoids) are further apart.

Equations (3a) and (4a) reduce to Eq. (2a) when f is small and $\sigma_\ell = 0$. Equations (3b) and (4b) reduce to Eq. (2b) when ϕ is small and $\sigma_h = \infty$ or $\rho_\ell = 0$ and the equations are rewritten in terms of ρ_m, ρ_ℓ and ρ_h, to avoid the infinities. However, Eq. (5) reduces to Eq. (1a) for all $f\,(1-\phi)$ if $\sigma_\ell = 0$, and to Eq. (1b) for all ϕ when Eq. (4) is rewritten in terms of ρ_m, ρ_ℓ, and ρ_h with $\sigma_h = \infty$ or $\rho_\ell = 0$. Therefore Eq. (5) predicts a metal-perfect insulator $(\sigma_m = 0)$ transition (MIT) when $f = \frac{2}{3}\,(\phi = \frac{1}{3})$ and $\sigma_\ell = 0$ and a perfect conductor-normal conductor $(\rho_m = 0)$ transition (PNT) when $\phi = \frac{1}{3}$ and $\rho_\ell = 0$. This behavior of $\sigma_m(\rho_m)$ characterizes the behavior at a percolation threshold, so the microstructure characterized by the BS theory displays a percolation type behavior. Eq. 5 is plotted as curve (d) in Fig. 2 for $A = 2(\phi_c = \frac{1}{3})$.

Figure 2 shows that the resistivities of media described by Eqs. (3) (lines b) and Eqs. (4) (lines c) are dominated by the host or matrix material until f or ϕ approaches 1. However, if there is a percolation type transition (or true percolation transition), as occurs in Eq. (5) (line d), the properties of the medium rapidly change from being dominated by one component to the other near ϕ_c, where $0 < \phi_c < 1$. The lines marked *a* in Fig. 2 are from the brick-layer model [11,12], which will be discussed later.

While the MW-HS equations give the outer limits of the resistivity (or conductivity) for isotropic media, an examination of Fig. 2 shows that the BA equation may well represent the practical inner limits for real microstructures, where there is a definite unbroken matrix, host or coating component. Should it be necessary, in order to fit a particular impedance spectrum, there are equations or models which give results which lie between the MW-HS and BA models. The first is the model in Merideth and Tobias [3]. Unfortunately this only holds for low grain or bulk fractions, which is usually not the case for most ceramics, and therefore will not be further examined.

Another possibility is to use Eq. (3a,b) to calculate the conductivity for a coating component, which consists of the conducting (insulating) component impregnated with small spherical insulating (conducting) grains. The conductivity of this coating component can then be inserted into Eq. (3a,b) to calculate the final conductivity. For this interpolation model, each building block would look like a single block shown in Figs. 1(c)(i) and (ii). The volume fraction of the dispersed phase in the coating component and the final media can be adjusted to suit the particular circumstances. An example will be given later in the paper.

The single exponent GEM equation given by,

$$(1-\phi)(\sigma_\ell^{1/t} - \sigma_m^{1/t})/(\sigma_\ell^{1/t} + A\sigma_m^{1/t}) + \phi(\sigma_h^{1/t} - \sigma_m^{1/t})/(\sigma_h^{1/t} + A\sigma_m^{1/t}) = 0 \qquad (6)$$

where t is an exponent and $A = (1-\phi_c)/\phi_c$, can also be used. This equation was originally arrived at as an interpolation between the BA and BS equations. It reduces to the BS equation for $t = 1$ and all values of ϕ_c, which is $\frac{1}{3}$ $(A = (1-\phi_c)/\phi_c = 2)$ for an infinite array of spheres, as shown in Fig. 1(a) (i) and (ii).

For $\sigma_\ell = 0$, $\phi_c = 0$ and $t = \frac{3}{2}$ the GEM equation is identical to the BA Eq. (4a), and for $\sigma_h = \infty$, $\phi_c = 1$ and $t = 3$ it is identical to the BA Eq. (4b). Note that for $t = 1$ and $\phi_c = 0$ it reduces to the addition of conducting slabs in parallel and for $t = 1$ and $\phi_c = 1$ it reduces to the addition of conducting slabs in series. These are the extreme values of the conductivity or resistivity for an anisotropic medium and lie outside curves *b* in Fig. 2 [2].

The brick-layer model, widely used in impedance spectroscopy, consists of cubic bricks arranged on a simple cubic lattice with the space between the bricks being filled with mortar [11]. Usually, in this model, the mortar is made to be rather thin and is more often a poor conductor compared to the brick material. However, the model can easily be solved [12] where there are thick, or even very thick, layers of mortar, which can be either more or less conducting than the brick material. In order to derive the general case, from a conductivity point of view, the building block of the system can be considered as a square pipe of mortar material, with the outside length equal to the size of the unit cell (i.e., 1) enclosing a parallelepiped with a cross-section equal to that of the brick, and unit

length [12]. Note the wall thickness of the square pipe is one half that of the actual mortar layer. Along the length of the square cross-sectioned parallelepiped are alternate layers of brick and mortar. Each parallelepiped contains a single brick with two mortar caps, each one half of the actual mortar thickness. The conductivity of the square pipe can be calculated directly, but the conductivity of the alternate layers of brick and mortar must be added using the reciprocal addition formula. The conductivities of the mortar pipe and brick-mortar parallelepiped can then be added as they are in parallel. If the edge of the brick is D and the thickness of the mortar layers is d $(D + d = 1)$, then the conductance of the pipe is $G(pipe) = \sigma(mor)\,x\,(1 - D^2)$ and for the parallelopiped $G(layers) = \sigma(mor)\,x\,\sigma(bri)\,x\,D^2/(\sigma(bri)\,x\,d + \sigma(mor)\,x\,D)$ respectively, which gives for the total conductance or conductivity (as the cell is of unit size) [12],

$$\sigma_{bricklayer} = \sigma_m = \sigma_{mor}(1 - D^2) + \sigma_{mor}\sigma_{bri}D^2/(\sigma_{bri}d + \sigma_{mor}D) \qquad (7)$$

In this formula either $\sigma_h = \sigma_{bri}$ and $\sigma_\ell = \sigma_{mor}$ or visa versa. The two solutions are plotted as curves *a* in Fig. 2. Note that the cubic symmetry of the BL model ensures that the conductivity is isotropic. Therefore, where it lies outside of the MW-HS limits it is fundamentally wrong.

Note that in deriving this formula it is assumed that all current in the pipe remains in the pipe and all current in the parallelepiped remains in the parallelepiped. This is obviously not the case in practice as the current will distort around the edges of the brick cubes. The effect is minimal when the mortar layers are very thin.

From Fig. 1 and the geometry of the brick-layer model it is obvious that Eqs. (2), (3) and (4) are only valid for systems where one component coats the other and the critical volumes are all 1, 0 or very close to these values. Should the coated (granular or dispersed) grains make contact with each other at volume fractions other than 0 or 1 [10], the appropriate equations are those from percolation theory [1,2,4–9] or the two exponent GEM Eq. [13–15]. However, for specific microstructures (Fig. 1), since it is an EM theory, the Bruggeman symmetric medium equation (Eq. 5) will be the correct equation.

3. Extensions to Multiphase Composites

The easiest extension, both visually and mathematically, is the BS model described by Eq. (5). The most general equation is

$$\sum_n (\phi_n(\sigma_n - \sigma_m)/(\sigma_n + A\sigma_m)) = 0 \qquad (8)$$

where ϕ_n is the volume fraction of the nth component and σ_n its conductivity. For $A = 2$, the medium consists of a mixture of n sets of spheres of different conductivity, each with an infinite range of sizes, randomly mixed in the correct ratio so that the spheres of similar sizes are well separated. Extensions to non-spherical, ellipsoidal building blocks can be made. This, as described earlier, requires a different value for A. As media which can be described by Eq. (8) or even Eq. (5) are not common, this extension will not be taken any further.

For both MW and brick-layer structures, it is easy to compute the conductivity of a system which has a further thin coating layer on a sphere or cube of a composite of known conductivity. This is accomplished by computing the conductivity of the inner sphere or cube of the new composite, using the appropriate volume fraction and conductivities in Eq. (3), and then putting this conductivity into Eq. (3) for the MW case and Eq. (6) for the brick-layer case, as the granular, dispersed, or coated fraction. This procedure can also be used to incorporate electrode effects into a computation. However, the usual arrangement for impedance spectroscopy is a parallel plate capacitor configuration. Therefore, the logical way to incorporate an electrode effect is to add a complex ''electrode'' resistance in series. This is done using the formula,

$$\sigma_{me} = 1/(v_m/\sigma_m + (1 - v_m)/\sigma_e) \qquad (9)$$

where σ_{me}, σ_m and σ_e are the conductivities of the medium and electrode in series, the effective medium and the electrode, respectively, while v_m is the volume fraction of the media between the electrodes.

Another interesting combination, due to Sheng [16], is where the coating component in a MW medium (Eq. 3) is constructed from a two-component BS medium. Such a coating component may be realistic for some ceramics and, in particular, cemented sedimentary rocks. As both phases in a spherical BS medium are continuous in the range $\frac{1}{3} < \phi < \frac{2}{3}$, this structure allows the continuous solid

cement component to bind the rocks, so that they have structural integrity and can propagate sound. At the same time a continuous fluid component can continue to slowly carry out the cementation process and carry a significant electric current compared with the other two solid components.

4. Results from Computer Simulations

In order to demonstrate that the above equations produce the type of impedance spectra observed in practice, a number of computer simulations are given below. Note that all the equations given above have been written in terms of the complex conductivity, whereas impedance spectra are usually plotted giving the imaginary component as a function of the real component of the impedance and sometimes the modulus, but very rarely as the admittance or capacitance. Therefore, in this paper the complex conductivity σ_m^*, as obtained from the above equations as a function of ω for fixed ϕ, was converted to the impedance or modulus using the following equations,

$$Z_{mr} = GF(\sigma_{mr}/(\sigma_{mr}{}^2 + \sigma_{mi}{}^2)) \text{ and}$$

$$M_{mr} = -\omega Z_{mi} \tag{10}$$

$$Z_{mi} = -GF(\sigma_{mi}/(\sigma_{mr}{}^2 + \sigma_{mi}{}^2)) \text{ and}$$

$$M_{mi} = \omega Z_{mr} \tag{11}$$

Here, GF is a geometric factor used to convert from conductivity to conductance, etc. In this paper GF is chosen so that the impedance or modulus given are for a one centimeter cube of material.

The simulations plotted in the following figures are all for a two-component system, where the more conducting component has $\sigma_h = 3 \times 10^{-5}(\text{ohm-m})^{-1}$, $\varepsilon_0\varepsilon_r = 3 \times 10^{-11}$ (Farad/m) or $\sigma_{hi} = 3 \times 10^{-11}\omega$, and a characteristic ω_h of 1×10^6; the more insulating one has $\sigma_l = 3 \times 10^{-8}(\text{ohm-m})^{-1}$ and $\varepsilon_0\varepsilon_r = 3 \times 10^{-11}$ (Farad/m), or $\sigma_{li} = 3 \times 10^{-11}\omega$, and a characteristic ω_1 of 1×10^3. These parameters lie in the range where IS is practical and, in some instances, allow two well-separated arcs to be observed. In order to obtain complete arcs (when two arcs were observed), ω was allowed to vary between 1 and 10^9. The latter frequency is higher than is usually used in practice. The above choice of conductivity parameters usually led to perfectly semi-circular arcs. If the conductivity Eq. [17,18] that produce depressed arcs for each of the two components are used, then depressed arcs are, of course, observed in all the simulations given below. By using single relaxation-time components in the present work it was possible to check for any arc distortions arising from the underlying microstructures on which the above equations are based.

In Fig. 3 the Nyquist (Cole-Cole) plots are given, using the real Z_{mr} and imaginary Z_{mi} impedances obtained from Eqs. (3), (4) and (7) using the above parameters, together with a volume fraction (ϕ) of 0.01, in the case where conductor coats the more insulating spheres (i.e., a conductor matrix system). Notice how close the results from the Maxwell-Wagner and brick-layer equations lie. Eq. (3) gives a far higher dc resistance than Eq. (4), in agreement with Fig. 2. We observed that the peak ω of the semi-circular arcs characterizing these conductor matrix media moves from 10^3 to 10^6 as the volume fraction of the conductor increases. As no interesting impedance arcs are obtained for higher volume fractions of an all-dominating conducting matrix, no more of these are presented.

If plots of Z_{mi} against Z_{mr} and M_{mi} against M_{mr} are made with the more insulating material as host or matrix, for all volume fractions, it becomes obvious that the modulii plots give more information in the form of double arcs over a larger range of volume fractions than the impedance plots. In both $Z_{mi} - Z_{mr}$ and $M_{mi} - M_{mr}$ plots, where two arcs are observed, they are almost perfect semi-circles with the ω characteristic of each component lying at the

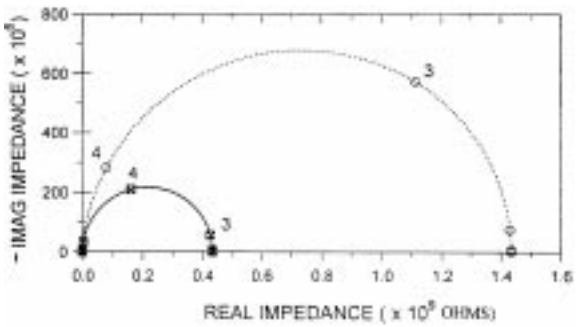

Fig. 3. The imaginary impedance ($-Z_{mi}$) plotted against the real impedance (Z_{mr}) using the MW (—), BA (.....) and ''bricklayer'' (– – – – –) equations, with $\phi = 0.01$. The conducting component has $\sigma_h = 3 \times 10^{-5}(\text{ohm-m})^{-1}$ and $\varepsilon_o\varepsilon_r = 3 \times 10^{-11}$ (Farad/m) and the insulating component $\sigma_l = 3 \times 10^{-8}(\text{ohm-m})^{-1}$ and $\varepsilon_o\varepsilon_r = 3 \times 10^{-11}$ (Farad/m). The exponent of ω is given at certain key points on the plots.

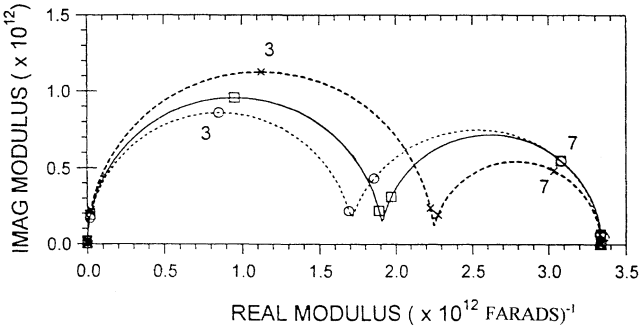

Fig. 4. The imaginary modulus (M_{mi}) plotted against the real modulus (M_{mr}) using the MW (—), BA (.....) and ''brick-layer'' (– – – – –) equations, with $\phi = 0.20$. The conducting component has $\sigma_h = 3 \times 10^{-5}$(ohm-m)$^{-1}$ and $\varepsilon_o \varepsilon_r = 3 \times 10^{-11}$ (Farad/m) and the insulating component $\sigma_l = 3 \times 10^{-8}$(ohm-m)$^{-1}$ and $\varepsilon_o \varepsilon_r = 3 \times 10^{-11}$ (Farad/m). The exponent of ω is given at certain key points on the plots.

associated maximum value of the imaginary impedance (modulus), as they should for components with a single relaxation time. No arcs are obtained for $Y_{mi} - Y_{mr}$ and $\varepsilon_{mi} - \varepsilon_{mr}$ plots.

Figure 4 shows plots of real M_{mr} against imaginary M_{mi} for a conducting volume fraction of 0.2. Here the important features are that, as expected, the MW and brick-layer plots no longer coincide and the peak of the high frequency arc is not at 10^6. Note that for this value of ϕ, an impedance plot does not give separated arcs.

Figures 5 and 6 show impedance plots for the conductor volume fractions of 0.99 and 0.90, respectively. The MW microstructure characterizing

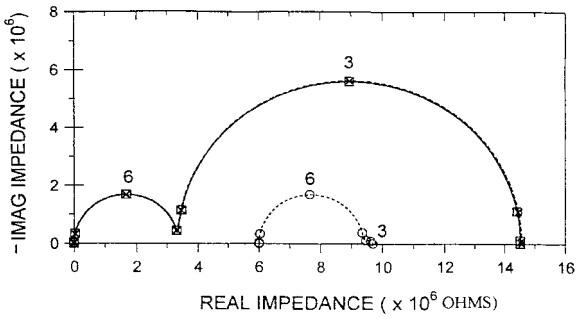

Fig. 5. The imaginary impedance ($-Z_{mi}$) plotted against the real impedance (Z_{mr}) using the MW (—), BA (.....) and ''brick-layer'' (– – – – –) equations, with $\phi = 0.99$. The conducting component has $\sigma_h = 3 \times 10^{-5}$(ohm-m)$^{-1}$ and $\varepsilon_o \varepsilon_r = 3 \times 10^{-11}$ (Farad/m) and the insulating component $\sigma_l = 3 \times 10^{-8}$(ohm-m)$^{-1}$ and $\varepsilon_o \varepsilon_r = 3 \times 10^{-11}$ (Farad/m). The exponent of ω is given at certain key points on the plots. Note that the BA plot has been shifted away from the origin to facilitate comparison with the other curves.

Fig. 5 ($f = 0.01$) is the easiest to visualize, as it consists of a large range of conducting spheres, each with a thin (0.003344 of the total radius) insulating coating. If the volume fraction (f) of the insulating layer is increased from 0.01 to 0.02, the width of the low frequency arc (in ohms) doubles and if f is decreased to 0.005, the original width of this arc halves. In both cases the width of the high frequency arc stays almost constant as the actual volume of this component barely changes. These changes are exactly what one would expect.

If the parameters for the high conductivity (interior) region are decreased to $\sigma_h = 1 \times 10^{-5}$(ohm-m)$^{-1}$ and $\varepsilon_0 \varepsilon_r = 1 \times 10^{-11}$ (Farad/m), so that the characteristic ω remains at 10^6 rad/s, the width of the arc characterizing the conducting medium increases by a factor of 10, due to the increased impedance. On the other hand, if the parameters for the high conductivity medium are increased to $\sigma_h = 1 \times 10^{-4}$ (ohm-m) and $\varepsilon_0 \varepsilon_r = 1 \times 10^{-10}$ (Farad/m), so that the characteristic $\omega = 10^6$ rad/s remains the same, the width of the high frequency arc decreases by a factor of ten, becoming just visible on the scale of Fig. 6. In all cases the value for the ω characterizing each medium remains at the top of the arc. These observations are obviously consistent with the changes made in the parameters. The brick-layer model plots are again in good agreement with the MW plots, due to the low f value of the mortar.

For comparison purposes, the Bruggeman Asymmetric model has been shifted away from the origin in Fig. 5. The shifted BA arc has a very similar high conductivity arc and a vanishingly small low conductivity arc. This suggests that in this BA

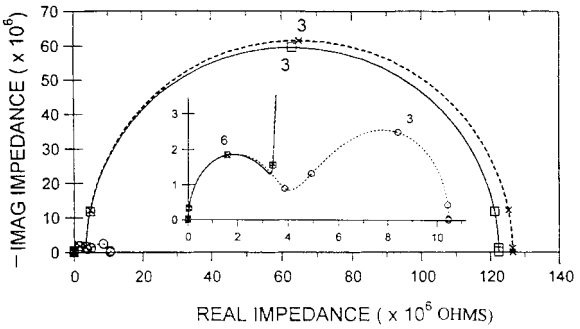

Fig. 6. The imaginary impedance $(-Z_{mi})$ plotted against the real impedance (Z_{mr}) using the MW (—), BA (.....) and ''brick-layer'' (– – – – –) equations, with $\phi = 0.90$. The conducting component has $\sigma_h = 3 \times 10^{-5}(\text{ohm-m})^{-1}$ and $\varepsilon_o \varepsilon_r = 3 \times 10^{-11}$ (Farad/m) and the insulating component $\sigma_l = 3 \times 10^{-8}(\text{ohm-m})^{-1}$ and $\varepsilon_o \varepsilon_r = 3 \times 10^{-11}$ (Farad/m). The exponent of ω is given at certain key points on the plots. The inset diagram is an enlargement of the high frequency region.

microstructure the infinite size range of conducting spheres must lie much closer to each other than in the MW microstructure, and effectively short-out the insulating medium. This would appear to be consistent with the microstructures shown in Fig. 1.

Figure 6 shows that when 0.1 volume fraction of the insulating medium coats the conducting spheres, the contribution of the conducting spheres to the impedance is nearly negligible for the MW microstructure and the brick-layer model. The plots for the MW equation and brick-layer model are now only in reasonable agreement. However, the insert again shows that, even at this volume fraction, the conducting spheres in a BA microstructure still lie close enough together to give a relatively negligible contribution to the impedance vis-à-vis the MW microstructure.

As the MW media equations and structure are equivalent to the Hashin-Shtrikman upper and lower bounds for an isotropic medium, the low frequency arcs in Figs. 5 and 6, due to the insulating component, are the maximum width (resistivity) obtainable for this component. The fact that the arcs due to the high conductivity component are similar for the MW and BA media is due to the fact that the current must maximize its path in this component in order to obtain the required minimum resistance. The very different arcs for the low conductivity component in the MW and BA media show that the size of the low conductivity component arc depends critically on microstructure, even in media where the low conductivity component obviously coats the high conductivity component.

Formulae which give results intermediate between the MW-HS and BA equations were described above. In Fig. 7 the impedance arcs resulting for these equations, using the same conductivities for the components as before, are given for $\phi = 0.99$ and so are to be compared with Fig. 5. For the media obtained by using Eq. (3b) twice, with $\phi = 0.9$ each time (total $\phi = 0.99$), is given by the short dash line, hereafter referred to as the insulator sphere impregnated coating model. All other lines are calculated using the GEM equation (Eq. 6), with $\phi_c = 0.999999999999$ (to avoid the infinity). The outer solid line curve, where a large semicircular arc terminates at a real impedance of 21 Mohm, is for $t = 1$ and is larger than the MW-HS value of 14.6 Mohm (Fig. 5). The long dash curve is for $t = 1.5$ and the inner solid curve is for $t = 3$. As in Fig. 5 the arc for the conducting material is virtually the same in all cases, again indicating that the difference in the low frequency impedance arcs between the models is governed by how effectively the microstructure of the insulating component separates the conducting spheres. Note that the $t = 3$ curve is similar to the BA curve (Fig. 5), as is to be expected since they are identical when $\sigma_\ell = 0$. The possible values of the exponents in the BA equations, based on the geometry of the grains, are discussed in

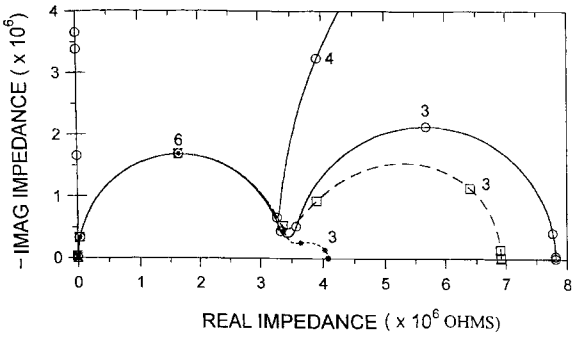

Fig. 7. The imaginary impedance $(-Z_{mi})$ plotted against the real impedance (Z_{mr}) using the insulator sphere impregnated coating model, described in the text and given by the short dash line; also Eq. (6) (GEM model) with $t = 1$ (upper solid line), $t = 1.5$ (long dash line) and $t = 3$ (lower solid line) for $\phi = 0.99$. The conducting component has $\sigma_h = 3 \times 10^{-5}(\text{ohm-m})^{-1}$ and $\varepsilon_0 \varepsilon_r = 3 \times 10^{-11}$ (Farad/m) and the insulating component $\sigma_l = 3 \times 10^{-8}(\text{ohm-m})^{-1}$ and $\varepsilon_0 \varepsilon_r = 3 \times 10^{-11}$ (Farad/m). The exponent of ω is given at certain key points on the plot.

Merideth and Tobias [3]. Unfortunately, a t of less than 3 is not permitted in the 3D BA model. Therefore for exponents less than three this model is one without a characterizable microstructure.

At the other extreme of the volume fraction, when $\phi = 0.01$, the following results were observed, but not shown in a figure. Equation (6), with $\phi_c = 1 \times 10^{-12}$ (to avoid the infinity for $\phi_c = 0$), gives a semi-circular arc for all t values. For $t = 1$, which when A is infinity ($\phi_c = 0$) is equivalent to adding conductivities in parallel and an anisotropic microstructure of alternate slabs in parallel, the low frequency real impedance is 280 Mohms, which is, as to be expected lower than the isotropic MW-HS value of 430 Mohm (Fig. 3). For $t = 1.5$ the real impedance is 820 Mohm and for $t = 3$ it is 138 Mohm.

The model, where the conducting coating component is one already impregnated with insulating spheres and, as has already been described, consists of using the MW-HS equation twice, with $\phi = 0.1$ each time to give a final φ of 0.01, gives a real impedance of 575 Mohm. This value lies closer to the MW-HS value of 430 Mohm than the BA value of 1420 Mohm.

One conclusion of this paper is that the presence of smaller coated particles between the bigger ones lowers the resistivity for the insulator matrix/host situations and increases it for the conductor host situations. Therefore, if the MW-HS model is not correct and if the results turn out to lie between the MW-HS and BA models, then after a careful examination of the microstructure and the grain or bulk size distribution, a model involving multiple use of the MW-HS equation may work. This, as previously described, would involve dividing the total grain volume into appropriate large and small volume fractions.

Note that the equivalent circuit for the MW media has been derived by Bonanos and Lilley [19] for a thin coating of insulator on conducting spheres and turn out to be two parallel RC elements in series with each other.

From the above and other simulations it can be seen that the brick-layer model and the MW equations, in spite of their very different ''microstructures'', give similar results for small volume fractions but when ϕ is close to 0.5 the results can differ by up to 50%. One reason for this difference is the fact that the current will, in practice, distort around the sharp edges of the bricks, which is not taken into account in the bricklayer model. This error would, of course, be largest when the thickness of the layers and lengths of the bricks are similar in size. Note that the BL and MW-HS models both have a conducting layer thickness that, for a given volume fraction, is a constant fraction of the cube edge or the sphere diameter, whereas a constant layer thickness irrespective of the grain size is often observed. In practice, the other problem with the BL model is the constant grain size and square corners, while the other problem with the MW-HS model is the infinite range of sphere size and perfectly round ''corners.'' However, the fact that the results from these two models agree so closely, for low or high ϕ values, indicates that the above problems are not as serious as one may think and that they are both reasonably valid models for certain classes of real media.

The results for simulated IS spectra, using the BS equation (Eq. 5) on systems with the same two components ($\sigma = 3 \times 10^{-5}$ and 3×10^{-8}(Ohm-m)$^{-1}$ and a common $\varepsilon_0\varepsilon_r$ of 3×10^{-11} (Farad/m)) as above, were also investigated. The $Z_{mi} - Z_{mr}$ and $M_{mi} - M_{mr}$ curves obtained for $\phi > \frac{1}{3}$ are virtually perfect single arcs, with the peaks characterized by the characteristic frequency of the major component. The plots given in Fig. 8 are $M_{mi} - M_{mr}$ for $\phi = 0.20$, $\frac{1}{3}$ and $\frac{2}{3}$. The volume fraction 0.20 was chosen as it gives a double arc similar to those in Fig. 4. This is not too surprising because, at this value of ϕ, the system consists of clusters of conducting spheres completely surrounded (coated) by insulating spheres. As in the MW, BA and brick-layer simulations, a double arc is not seen for a

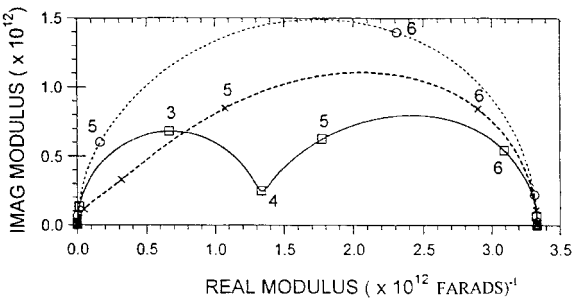

Fig. 8. The imaginary modulus (M_{mi}) plotted against the real modulus (M_{mr}) using the BA equation, with $\phi = 0.20$ (—), $\frac{1}{3}$ (.....) and $\frac{2}{3}$ (– – – – –). The conducting component has $\sigma_h = 3 \times 10^{-5}$(ohm-m)$^{-1}$ and $\varepsilon_o\varepsilon_r = 3 \times 10^{-11}$ (Farad/m) and the insulating component $\sigma_l = 3 \times 10^{-8}$(ohm-m)$^{-1}$ and $\varepsilon_o\varepsilon_r = 3 \times 10^{-11}$ (Farad/m). The exponent of ω is given at certain key points on the plots.

$Z_{mi} - Z_{mr}$ plots at $\phi = 0.20$. The other two volume fractions were selected because the high conductivity component becomes continuous at $\phi = \frac{1}{3}$ and the insulating component becomes discontinuous at $\phi = \frac{2}{3}$. Between $\phi = \frac{1}{3}$ and $\frac{2}{3}$ both components have continuous percolation channels. What can be seen from these curves and other curves is that this medium shows both depressed and distorted arcs, especially near $\phi = \frac{1}{3}$, due only to this particular geometrical arrangement of the conducting components. Below $\phi = \frac{1}{3}$ and above $\phi = \frac{2}{3}$, the depression and distortions decrease so that at $\phi = 0$ and 1 perfect semi-circular arcs are obtained. Note that the medium is always isotropic and the depression and distortion of the arc depends on the relative values of the conductivity of the two components.

Another case where a depressed arc was obtained from the nature of the shape or distribution of the conducting components was where the MW model was extended to randomly oriented, but coated (MW medium), ellipsoids of rotation [20], i.e., still a macroscopically isotropic medium. Therefore, in the interpretation of IS spectra the depression of an arc, or arcs, due to particular or peculiar arrangement of crystal shapes and distributions of coated components cannot be ruled out, even though the two components, grain and coating, may each have a single characteristic frequency.

5. Equivalent Circuit Fitting

Experimental impedance data are often analyzed in terms of equivalent circuits involving resistors and capacitors. Several commercial software packages, e.g., ''Equivalent Circuit'' [21], allow deconvolution of individual R, C elements. We applied ''Equivalent Circuit'' to the EM model spectra in the present work. With the exception of the BS spectra between the percolation thresholds, we consistently obtained well-behaved fits involving combinations of usually one or two RC elements (resistor and capacitor in parallel) which are further connected in series, (RC)(RC) or parallel, ([RC][RC]), employing ''Equivalent Circuit'' notation [21]. It should be stressed that, with the exception of the distorted BS arcs in Fig. 8, little or no arc depression or distortion due to the microstructure was observed (Figs. 3–7).

What is troubling about the equivalent circuit fits obtained is that the component values obtained are as much a function of the microstructure as they are of the complex conductivities of the composite components. This can be seen in Table 1, where the number of Z-arcs, M-arcs, and the ratio of low frequency-to-high frequency capacitance and resistance are tabulated. The latter values were obtained from Bode plots of total capacitance or impedance vs. frequency. Resistance ratios are reported only for cases where two plateaus were clearly visible in the impedance Bode plot. It should be kept in mind that an identical real permittivity was employed for each component in the EM modeling and that the conductivities differ by 1000. The significant low frequency capacitance in the case of MW-HS and BL models (with insulating coatings) is therefore due to the microstructure, i.e., at low frequencies the thin coatings (or grain boundaries) give rise to large capacitors. Note too the divergence of the MW-HS and BL equivalent circuits as the volume fraction of the coating (grain boundary) phase increases. It must therefore be stressed that without independent knowledge of the microstructure, e.g., second phase volume fraction, distribution, thickness, etc., which would enable one to calculate an effective geometrical constant for the impedance of each component, it is impossible to derive the correct complex conductivity for each component from equivalent circuit fitting of spectra. This has important ramifications for the interpretation of experimental impedance spectra in that one cannot obtain quantitative microstructure and conductivity parameters for the components from an equivalent circuit analysis alone.

It can be observed that even higher low frequency capacitances are observed for the BA model at the same insulator fractions as in the BL and MW-HS cases. This observation, combined with the comparatively smaller increases in low frequency resistance, must arise from the unique microstructure, which brings conductor particles much closer together than in those models.

6. Application to Experimental Electroceramic Systems

A system which closely approximates the BA model in terms of microstructure and impedance response is that of insulating sand particles in hardened cement paste (HCP), commonly referred to as ''mortar.'' HCP is a reasonably good ionic conductor, if fully saturated

Table 1. Equivalent circuit fitting for various models

Model description	No. Z-arcs	No. M-arcs	C(Lo)/C(Hi	R(Lo)/R(Hi)
BA C-0.01	1	1 + (or 2)	1.23	—
BA C-0.10	1	1 + (or 2)	1.46	—
BA C-0.20	1	1 + (or 2)	1.45	—
BA I-0.10	2 (or 2 +)	1	133.15	2.63
BA I-0.20	2	2	71.60	7.43

Model description	No. Z-arcs	No. M-arcs	C(Lo)/C(Hi)	R(Lo)/R(Hi)
BL C-0.01	1	1	1.01	—
BL C-0.10	1	1 +	1.03	—
BL C-0.20	1	1 +	1.07	—
BL I-0.01	2	2	176.35	4.36
BL I-0.10	2	2	25.44	36.05
BL I-0.20	2	2	11.82	70.97

Model description	No. Z-arcs	No. M-arcs	C(Lo)/C(Hi)	R(Lo)/R(Hi)
BS C-0.01	1	2	1.03	—
BS C-0.10	1	2	1.42	—
BS C-0.20	1	2 +	2.44	—
BS C-0.80	1	1	1.21	—
BS C-0.90	1	1	1.09	—
BS C-0.99	1	1	1.01	—

Model description	No. Z-arcs	No. M-arcs	C(Lo)/C(Hi)	R(Lo)/R(Hi)
MW-HS C-0.01	1	1	1.03	—
MW-HS C-0.10	1	1 +	1.33	—
MW-HS C-0.20	1	1 +	1.74	—
MW-HS I-0.01	2	1	176.66	4.35
MW-HS I-0.10	2	2	26.66	34.62
MW-HS I-0.20	2	2	12.64	66.47

BA: Bruggeman Asymmetric Model, BL: Brick Layer Model, BS: Bruggeman Symmetric Model, and MW-HS: Maxwell-Wagner (or Hashin-Shtrikman) Model. ''I-'' and ''C-'' indicate the type of the coating materials: ''I-'' for an insulating component and ''C-'' for a conducting component). Numbers indicate the volume fractions of the insulating or conducting components. (e.g., BA C-0.01: Bruggeman Asymmetric Model with a volume fraction of 0.01 in the case where the conductor coats the more insulating spheres (i.e., a conductor matrix system). A''+'' indicates the hint of an additional arc.

with water, by virtue of a highly conductive pore phase, and impedance spectroscopy has become an important tool to study microstructural evolution [22]. We can treat HCP as a homogeneous, conductive matrix phase, and add sand grains having a wide range of particle sizes to produce a microstructure which closely approximates the BA model in Fig. 1(c). Impedance spectra consist of a single impedance arc, as in Fig. 3 [23]. Furthermore, the dc (low frequency) conductivity closely follows Eq. (4a) versus volume fraction of sand, as shown in Fig. 9, the only exception being during early stages of hydration, where the temporary influence of a more conductive ''rim'' or ''interfacial transition zone'' on the sand grains makes a minor contribution [23]. At early times (prior to set, when the paste is a ''slurry'' of sand particles in a matrix of water and much smaller cement grains) and later times (well after set), this additional component can be neglected and the BA model is an excellent description of behavior (see Fig. 9).

Another application of the BA model involves porosity in highly porous, conductive, polycrystalline

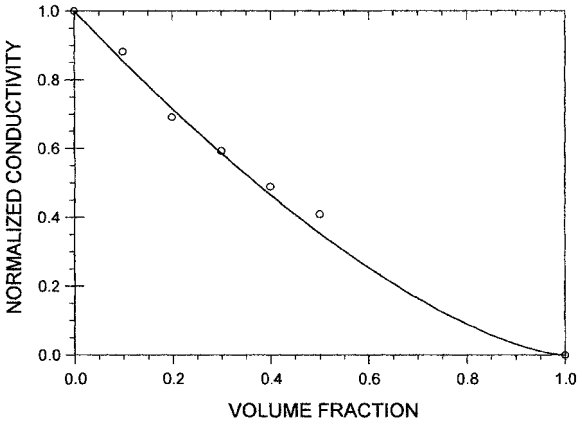

Fig. 9. Mortar (cement paste plus sand) conductivity normalized by paste conductivity vs. volume fraction of sand at 372 h of hydration [23]. The line corresponds to the Bruggeman Asymmetric model with a dispersed phase of zero conductivity.

ceramics. Given a relatively wide range of pore sizes and a disconnected pore network, the above results show that Eq. (4a) could be a good model description of composite conductivity at high overall levels of porosity, i.e., outside the dilute limit. Another model for this is Eq. (3a). In the dilute limit, i.e., porosity less than 10%, the results would not differ by much.

A system which approximates the BL or even the MW-HS microstructure with a highly conducting coating or grain boundary phase involves the solid state reaction of La_2O_3 and CuO to form La_2CuO_4 [24]. Impedance spectra consist of a single impedance arc, as in Fig. 3. Furthermore, the conductivity rises precipitously vs. volume fraction of La_2CuO_4 (the most highly conductive of the three phases) which was interpreted as Cu rapidly diffusing along the La_2O_3 particles where it reacts to form a 3D network of La_2CuO_4 [24]. Examples exist where grain boundaries in single-phase ceramics are more conductive than the grain cores (e.g., [25], based on point-probe dc studies of large-grained samples), however impedance measurements in such systems are usually not possible due to the small time constants $(R \times C)$ involved and the correspondingly high frequencies required (i.e., $>$ MHz).

On the other hand, there are numerous examples of ceramics with continuous and resistive grain boundary phases and/or space-charge layers, which are candidates to be modeled by the BL, MW-HS or BA equations. At this stage most systems have only been analyzed using equivalent circuits or the BL model. Examples of grain boundary-controlled electroceramics include varistors, positive temperature coefficient of resistance (PTCR) thermistors, boundary-layer capacitors, and even magnetic ferrites (with oxidized, high resistance grain boundaries to reduce eddy-currents). Studies of an electroceramic system, cerium dioxide, over a wide range of grain sizes, from nanometer to micrometer is reported in Hwang et al. [12]. For micrometer-grained material two distinct impedance arcs were obtained, as in Fig. 5, with each arc (grain interior and grain boundary) being well-behaved, i.e., little or no arc depression. Nanophase samples, however, exhibited much smaller resistivity ratios (grain boundary-to-grain interior), leading to vanishingly small grain boundary (low frequency) arcs. This is consistent with enhanced defect populations and transport characteristics associated with surfaces/grain boundaries in ceria [26,27].

A classic instance of grain boundary influence on immittance spectra involves the ionic conductor, yttria-stabilized zirconia (YSZ). Bonanos et al. [28] report a Nyquist plot (see Fig. 4.1.19(b) in [28]) for YSZ (6 m/o Y_2O_3) at 240°C, showing distinct bulk, grain boundary, and electrode (Pt) arcs. They also reported an SEM/TEM-derived ratio of grain boundary width-to-grain size ratio of approximately 10^{-3} (~ 10 nm vs. ~ 10 μm). In the MW-HS model, this would require $\phi = 0.994$. When fitting this data, using the MW-HS expressions, certain assumptions based on measured parameters are made. The first is that $\varepsilon_r = 12$ or $\varepsilon_r\varepsilon_o = 1.05 \times 10^{-10}$ (Farad/m) for the grains, which gives $\sigma_g = 1.1 \times 10^{-5}$ (ohm-m)$^{-1}$, if the 10^4 and 10^2 Hz theory and experimental points are to line up. If one assumes that ε_r is the same for the grain boundaries one obtains $\sigma_b = 5.5 \times 10^{-9}$ (ohm-m)$^{-1}$ and $\phi = 0.9991$, for the theoretical and experimental 10 and 1 Hz points to line up. $\phi = 0.9991$ corresponds to an effective electrical grain boundary thickness of 1.5 nanometers. This result is given in Fig. 10(a). If one assumes alternatively that $\phi = 0.994$ then $\sigma_b = 3.68 \times 10^{-8}$ (ohm-m)$^{-1}$ and $\varepsilon_r\varepsilon_o = 7.03 \times 10^{-9}$ (Farad/m) for the 10 and 1 Hz points to line up. The result using these parameters is given in Fig. 10(b). Based on an electrode volume fraction of 10^{-6}, a σ_e of 6.5×10^{-12} (ohm-m)$^{-1}$ and a $\varepsilon_r\varepsilon_o$ of 3.1×10^{-10} (Farad/m) give an arc in which the theoretical and experimental 10^{-2} points line up, as is

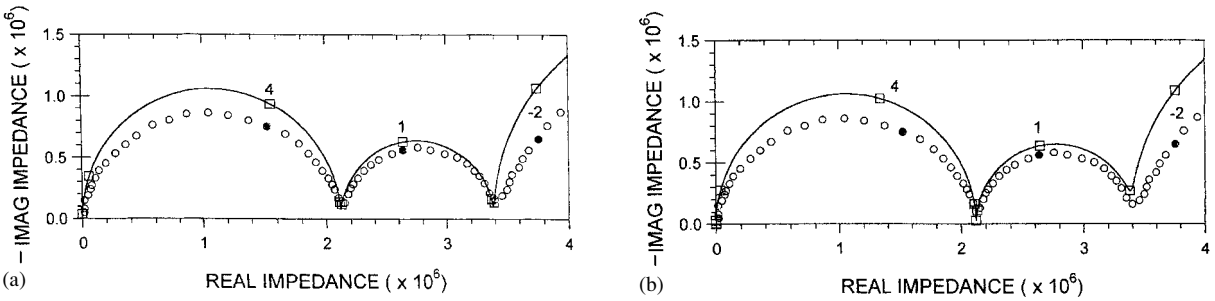

Fig. 10. Plots of the imaginary impedance $(-Z_{mi})$ against the real impedance (Z_{mr}). The circles are the experimental results for $ZrO_2(6\%Y_2O_3)$ at 240°C [28]. The solid lines are two different fits of the MW-HS equation and a series electrode resistor to these results. More details and the parameters used in are given in the text. The exponent of the frequency is given at certain key values by the squares and filled circles.

shown in Figs. 10 (a) and (b). (These values for the electrode—volume fraction and the electrical parameters—are quite arbitrary; any number of combinations are capable of simulating the electrode response.) Of these non-optimized fits, the first (fixed ε_r) is probably the better as the depths of the minima at 100 and 1 Hz are much closer to the experimentally observed minima than the second (fixed ϕ) case, where the theoretical minimum at 100 Hz is lower and the one at 1 Hz is higher than the experimental results. Note too that the theoretical curves are perfect semicircular arcs, as only a single relaxation time has been assumed, whereas the experimental data shows the usual arc depression.

It is surprising that the MW-HS fit quality depends upon the choice of fixed ε or fixed grain boundary thickness, since this should not be the case for the BL model (with negligible grain boundary thickness). This distinction between the two models could be important in deciding which is more valid given a high quality data set (known grain size and grain boundary thickness).

Not too surprisingly, considering the structure of the material, a fit of the same data to the BA equation does not work. A BA fit was done using a ϕ of 0.994 and the lowest possible $\varepsilon_r\varepsilon_o$ of 8.85×10^{-12} (Farad/m), which gives the minimum allowable grain boundary conductivity $(4.6 \times 10^{-11}(\text{ohm-m})^{-1})$, and maximum arc width, if the characteristic ω_c of the grain boundary material is to remain the same as in Fig. 10(b). The resulting arc is both distorted and depressed with a real zero frequency impedance of 3×10^6 ohms. It is obviously now essential to do an optimized fit on the original IS data of well characterized samples, determining and using the appropriate (optimum) expressions for the conductivities, inserting where possible separately measured conductivity and volume fraction parameters.

If they can be shown to fit and model the experimental data for certain ''coated grain'' systems, the BL, MW-HS, and BA models would have the advantage in that the actual complex conductivities and volume fractions of the components could be inserted or determined. In order to obtain a unique fit, it will almost certainly be necessary to insert reasonably accurate, independently determined fixed values for some parameters, such as the real dielectric constant and the volume fractions of ''phases,'' and to obtain the remainder from the fitting program. Where depressed arcs are observed, still further parameters will be needed.

The correct way and only way of fitting experimental data is to fit the data to the appropriate equation (with electrode effects if necessary), using the measured real and imaginary values as a function of frequency, for a given ϕ value. The inserted (fixed) and final fitted parameters can then be used to obtain the desired electrical response, such as impedance or modulus and a Nyquist plot of this quantity made.

7. Conclusions

Effective medium theories can be readily extended from dc to ac applications, such as impedance spectroscopy, by appropriate substitution of complex parameters (conductivity, dielectric constant, etc.) into the basic equations. Our consideration of the Maxwell-Wagner-Hashin-Shtrikman, Bruggeman

Asymmetric, Bruggeman Symmetric and brick-layer equations and their underlying microstructures leads to the follow conclusions:

- At low volume fractions of a conductive coating (matrix), the MW-HS and BL models yield virtually identical single-arc impedance spectra. Therefore they are equivalently good phenomenological representations for electroceramics with highly conductive grain boundaries or particle compacts with uniform and continuous coatings of the conductive phase.
- At low volume fractions of an insulating coating (matrix), the MW-HS and BL models yield virtually identical dual-arc impedance spectra. Therefore they are equivalently good phenomenological representations for electroceramics with resistive grain coatings (boundaries) or particle compacts with uniform and continuous coatings of insulating phase, if the volume fraction of the coating is small.
- As the MW-HS and BL models give virtually identical results in the low volume fraction (coating) matrix limit, whether the coating is conductive or insulating, this implies that the MW-HS equations can model systems where the range in the size of the coated spheres is not large.
- The BA model differs markedly from the MW-HS and BL models in the low fraction (coating) matrix limit, whether the coating is conductive or insulating, but especially so with an insulating coating. This shows that even when the coating is continuous (3D) the size and space distribution of the grain or spheres plays a role in determining the complex conductivity and the IS arcs. In the BA case, the closer proximity of conducting spheres to each other effectively shorts-out the insulating medium.
- At high volume fractions of a conducting matrix phase, the MW-HS and BA models both yield single-arc impedance spectra and are models for systems with isolated ''particles'' of insulating phase (e.g., porosity, residual ''parent'' particles in solid state reaction, sand grains in mortar, etc.). Which is the appropriate one must be determined by fitting the experimental arc and its frequency markers to either equation or an interpolation. DC conductivity results plotted against volume fraction is also useful in determining the appropriate model.
- In compacts or sintered specimens involving two phases, which do not coat or wet each other, the BS model is an appropriate starting point to describe the immittance responses and also conductivity vs. volume fraction behavior. However as, in most real or continuum systems of this nature, grains of nearly equal size come in contact with each other, it is usually necessary to use the percolation or one- or two- exponent GEM equations to describe the experimental results.
- Distinct dual-arc behavior is more often observed in modulus plots; it is strongly recommended that these be evaluated alongside impedance plots when attempting to interpret the immittance response of a given system.

Acknowledgments

This work was supported by the U.S. Department of Energy under grant no. DE-FG02-84-ER45097. DSM acknowledges receipt of an Eshbach Scholarship from the Northwestern University McCormick School of Engineering and Applied Science.

References

1. R. Landauer, in *Electrical Transport and Optical Properties of Inhomogeneous Media*, edited by J.C. Garland and D.B. Tanner. (AIP Conf. Proc. 40, New York, 1978), p. 2.
2. D.S. McLachlan, M. Blaszkiewicz, and R.E. Newnham, *J. Am. Ceram. Soc*., **73**, 2187 (1990).
3. R.E. Meredith and C.W. Tobias, in *Advances in Electrochemistry and Electrochemical Engineering* Vol. 2, edited by C.W. Tobias (Interscience, New York, 1962), p. 15.
4. D. Stauffer and A. Ahorony, *Introduction to Percolation Theory* (Taylor and Francis, London, 1994).
5. *Percolation Processes and Structures*, edited by G. Deutscher, R. Zallen and J. Adler, (Annals of the Israeli Physical Society, Vol. 5, Jerusalem, 1983).
6. G.W. Milton, in *The Physics and Chemistry of Porous Media,* edited by D.L. Johnson and P.N. Sen. (AIP Conf. Proc. 107, New York, 1983), p. 66.
7. D.J. Bergman and D. Stroud, in *Solid State Physics* Vol. 46 (Academic Press, San Diego, 1992), p. 147.
8. C.-W. Nan, *Prog. in Mat. Sci*., **37**, 1 (1993).
9. R. Zallen, *The Physics of Amorphous Solids* (John Wiley, New York, 1983) Chap. 4.
10. D.S. McLachlan, *Mat. Res. Soc. Symp. Proc*., Vol. **411**, (Materials Research Society, Pittsburgh, PA, 1996), p. 309.
11. M.J. Verkerk, B.J. Middlehuis, and A.J. Burgraaf, *Solid State Ionics*, **6**, 159 (1982).
12. J.-H. Hwang, D.S. McLachlan, and T.O. Mason, *J. Electroceram.*, **3**, 7 (1999).

13. J. Wu and D.S. McLachlan, *Phys. Rev*., **B56**, 1236 (1997).
14. J. Wu and D.S. McLachlan, *Phys. Rev*., **B58**, 14880 (1998).
15. D.S. McLachlan, W.D. Heiss, C. Chiteme, and Junjie Wu, *Phys. Rev*., **B58**, 13558 (1998).
16. P. Sheng, *Phys. Rev*., **B41**, 4507 (1990).
17. K.S. Cole and R.H. Cole, *J. Chem. Phys*., **9**, 341 (1941).
18. S. Harviliak, Jr and S. Neganu, *J. Polymer Science (Part C)*, **14**, 99 (1966).
19. N. Bonanos and E. Lilley, *J. Phys. Chem. Solids*, **42**, 943 (1981).
20. H. Friche, *J. Phys. Chem*., **57**, 934 (1953).
21. B.A. Boukamp, EQUIVCRT, Dept. of Chemical Technology University of Twente, P.O. Box 217, AE Enschede, The Netherlands, 1990.
22. B.J. Christensen, R.T. Coverdale, R.A. Olson, S.J. Ford, E.J. Garboczi, H.M. Jennings, and T.O. Mason, *J. Am. Ceram. Soc*., **77**, 2789 (1994).
23. J.D. Shane, T.O. Mason, H.M. Jennings, E.J. Garboczi, and D.P. Bentz, *J. Am. Ceram. Soc*., **83**, 1137 (2000).
24. E.A. Cooper, T.O. Mason, M.E. Biznek, and U. Balachandran, *J. Am. Ceram. Soc*., **73**, 154 (1990); E.A. Cooper and T.O. Mason, *J. Am. Ceram. Soc*., **78**, 857 (1995).
25. J. Jamnik, J. Fleig, and J. Maier, *Mat. Res. Soc. Symp. Proc*., Vol. **411** (Materials Research Society, Pittsburgh, PA, 1996), p. 25.
26. Y.-M. Chiang, E.B. Lavik, I. Kosacki, H.L. Tuller, and J.Y. Ying, *J. Electroceramics*, **1**, 7 (1997).
27. J.-H. Hwang and T.O. Mason, *Z. Phys. Chem*., **207**, 21 (1998).
28. N. Bonanos, B.C.H. Steele, E.P. Butler, W.B. Johnson, W.L. Worrell, D.D. Macdonald, and M.C.H. McKubre, in *Impedance Spectroscopy: Emphasizing Solid Materials*, edited by J.R. Macdonald (Wiley Interscience, New York, 1987) p. 217.